Electron. Mater. Lett., Vol. 12, No. 3 (2016), pp. 388-398
DOI: 10.1007/s13391-016-6002-8

Aromatic Substituents for Prohibiting Side-Chain Packing and π-π Stacking in Tin-Cored Tetrahedral Stilbenoids

Cheolmin Kim, Min-Ju Yoon, Seok Hee Hong, Minjoon Park, Kwangyong Park*, and Soo Young Kim*

School of Chemical Engineering and Materials Science, Chung-Ang University, Seoul 06974, Korea

(received date: 3 January 2016 / accepted date: 30 January 2016 / published date: 10 May 2016)

Tetrahedral structures comprising Sn-cored materials with five different types of substituents were synthesized. For the substituents, we employed methyl and *tert*-butyl as aliphatic groups, and naphthyl and phenyl as aromatic groups. The bandgap is in the range of 3.28 - 3.56 eV. The All the compounds with substituents showed bathochromical photoluminescence characteristics and exhibited aggregation-induced emission characteristics. Specifically, the compounds with aromatic substituents prohibited side-chain packing and π-π stacking. The energy levels of the highest occupied and lowest unoccupied molecular orbitals were measured to be 5.5 - 5.75 and 2.0 - 2.37 eV, respectively. The maximum luminance efficiencies and power efficiencies of the Sn-cored compound-based organic light-emitting diodes (OLEDs) were 0.38 - 0.71 cd/A and 0.15 - 0.28 lm/W. Therefore, it is expected that Sn-cored compounds with a tetrahedral structure, especially those containing aromatic substituents, can be used as an active material in blue OLEDs for prohibiting side-chain packing and π-π stacking.

Keywords: organic light emitting diode, tin-cored, aromatic substituents, π-π stacking

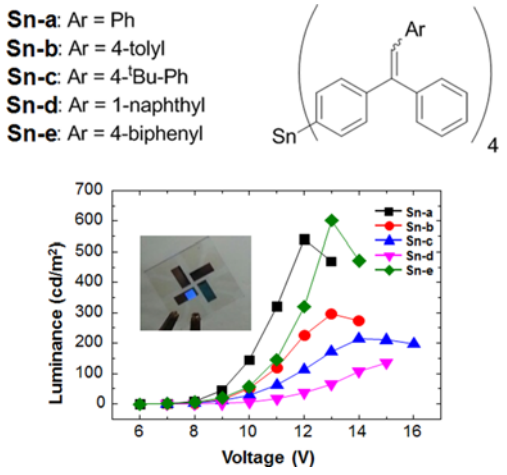

1. INTRODUCTION

Organic light-emitting diodes (OLEDs) have received considerable attention as next-generation displays and solid-state lighting sources owing to their low driving voltage, low power consumption, high contrast ratio, fast response time, high color rendering, and low cost.[1-4] Efficient blue-, green-, and red-emitting materials are necessary for full color displays or white emission. However, blue OLEDs have problems-such as a low stability, poor color purity, and low efficiency compared with red and green OLEDs-due to the poor quality of the organic materials, their wide bandgap, and the lack of research concerning their optimization.[5,6]

Derivatives of distyrylarylene, bistriphenylenyl, diarylfluorene/spirobifluorene, fluorene, pyrene, fluoranthene, and anthracene/diarylanthracene have been investigated for the synthesis of non-doped host materials for blue OLEDs. Among these, distyrylarylene derivatives with stilbene components are generally adopted as blue fluorescent materials.[7] However, distyrylarylene derivatives exhibit a tendency of crystallization because of their close intermolecular chromophoric π-π stacking, which induces a short lifetime and emission quenching in OLED applications.[8,9] Thus, tetrahedral,[10-12] dendron,[13,14] hyperbranch,[15,16] spir,[17] and unsymmetrical[7,18] structures have been investigated to prevent the chromophoric π-π stacking, although these structures are not free from aggregation. It is reported that luminogens, which exhibit weak or no emission in dilute solutions, exhibit strong light in the aggregates; this is called aggregation-induced emission (AIE).[19-23] Therefore, we consider that organic molecules with a tetrahedral structure and the AIE property are adequate OLED materials to prevent the chromophoric π-π stacking.

In this study, we investigated the effect of the functional

*Corresponding author: kypark@cau.ac.kr
*Corresponding author: sooyoungkim@cau.ac.kr

group of Sn-cored tetrahedral stilbenoids on the OLED performance. The core metal was used for the Sn because it requires four oxidation numbers to form a tetrahedral structure. Stilbenoid components were adopted for making blue OLEDs. The aliphatic (methyl and *tert*-butyl) and aromatic (naphthyl and phenyl) substituents were used as functional groups of the Sn-cored tetrahedral stilbenoids. The materials were synthesized by a protection and deprotection reaction of the carbonyl groups, a Horner-Wadsworth-Emmons reaction, and a halogen-lithium exchange reaction. Compounds with five different functional groups were synthesized, including tetrakis(4-(1,2-diphenylvinyl) phenyl)stannane (Sn-a), tetrakis(4-(1-phenyl-2-(4-tolyl)vinyl) phenyl)stannane (Sn-b), tetrakis(4-(4-(4-*tert*-butylphenyl)-1-phenylvinyl)phenyl)stannane (Sn-c), tetrakis(4-(2-(naphthaalene-1-yl)-1-phenylvinyl)phenyl)stannane (Sn-d), tetrakis(4-(2-(biphenyl-4-yl)-1-phenylvinyl)phenyl)stannane (Sn-e), and tetrakis(4-(2-(4-bromophenyl)-1-phenylvinyl) phenyl)stannane (Sn-f). Material characteristics such as the bandgap, energy level, and crystallinity were measured to investigate the effect of the tetrahedral structure. The application of Sn-cored stilbenoids materials as an OLED emitting layer is discussed.

2. EXPERIMENTAL PROCEDURE

2.1 General

All reactions were conducted under an inert Ar atmosphere. The solvents-tetrahydrofuran (THF), Et_2O, and dioxane-were distilled from an appropriate drying agent-sodium benzophenone ketyl-prior to use. Commercially available reagents were used without further purification, unless otherwise stated. ^{1}H NMR (300 or 600 MHz) and ^{13}C NMR (75 or 150 MHz) were recorded in $CDCl_3$ as solvent, using tetramethylsilane (TMS) as an internal standard, unless otherwise stated. Chemical shifts are reported in δ units (ppm) by assigning the TMS resonance in the ^{1}H NMR spectrum as 0.00 ppm and the $CDCl_3$ resonance in the ^{13}C spectrum as 77.2 ppm. All coupling constants, J, are reported in hertz (Hz). Flash column chromatography was performed on silica gel 60, 70 - 230 mesh. Analytical thin-layer chromatography (TLC) was performed using Merck Kieselgel 60 F254 pre-coated plates with a fluorescent indicator and visualized with ultraviolet (UV) light (254 and 365 nm in wavelength) or by iodine vapor staining. A gas chromatography (GC) analysis was performed on a bonded 5% phenyl-polysiloxane BPX five-capillary column (SGE, 30 m, 0.32 mm i.d.). Electron impact (EI, 70 eV) was used as the ionization method for the mass spectrometry. Mass data are reported in mass units (m/z). The mass data of the final products with a high molecular weight were collected by a matrix-assisted laser desorption ionization-time of flight (MALDI-TOF) mass spectrometer. The melting points were determined, and the uncorrected values are reported. The absorption and emission spectra were obtained using JASCO V-670 and PSI Darsa Series-740, respectively. The UV-visible (UV-Vis) absorption (V-670 UV-vis spectrophotometer) and photolumines cence (QuantaMaster/PTI) (PL) spectra were measured to confirm the optical properties. Synchrotron radiation photoelectron spectroscopy experiments were performed in an ultra-high-vacuum chamber (base pressure of ~10^{-10} Torr) at the 4D beamline of the Pohang Acceleration Laboratory. The onset of the photoemission was measured using incident photon energy of 90 eV and a negatively biased sample. The results were corrected using an Au internal reference to eliminate charging effects. A two-dimensional grazing incident X-ray diffraction (2D-GIXD) analysis was performed at the 3C beamline of the Pohang Acceleration Laboratory.

2.2 Synthesis scheme

The synthesis scheme is shown in Fig. 1. Tetrakis(4-(5,5-dimethyl-2-phenyl-1,3-dioxan-2-yl)phenyl)stannane (**3**) was prepared by the reaction of tin(IV) chloride with four equivalents of 2-(4-bromophenyl)-5,5-dimethyl-2-phenyl-1,3-dioxane, prepared from 4-bromobenzophenone (**1**), in the presence of *n*-butyl lithium (*n*-BuLi). The tetraketalstannane (**3**) was purified by recrystallization in ether to yield 91% isolated pure white powder. The acid-catalyzed deprotection of (**3**) was conducted using p-TsOH generated tetrakis(4-benzoylphenyl)stannane (**4**) as a clear crystalline solid in a 90% isolated yield after a facile recrystallization in Et_2O. Tetrakis(4-(1,2-diphenylvinyl)phenyl)stannanes (**6**) were prepared through the reactions of tetraketone (**4**) with four

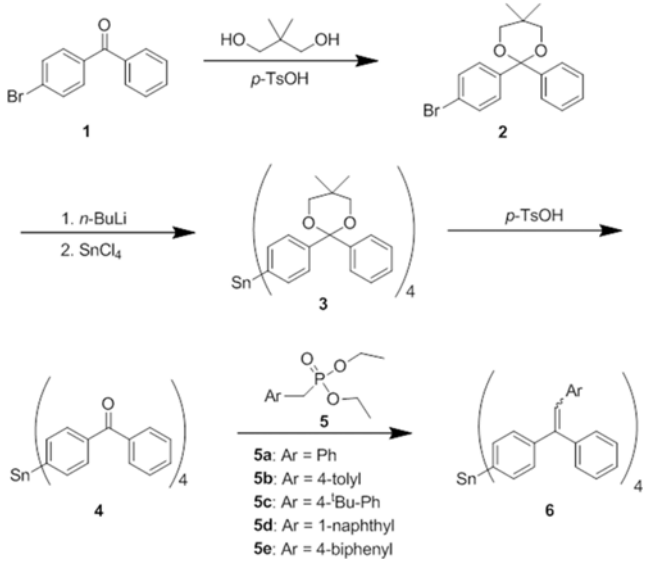

Fig. 1. Synthesis scheme for Sn-cored organic compounds. Methyl, *tert*-butyl, naphthyl, and phenyl were used as substituents for Sn-b, c, d, and e, respectively.

equivalents of benzylphosphonates (**5**) by constructing the central vinyl moiety of the stilbene structure. All phosphonates efficiently reacted with the ketone moiety in good yields (Sn-a: 83%, Sn-b: 80%, Sn-c: 82%, Sn-d: 73%, Sn-e: 68%). The detailed synthesis steps are explained as follows.

Preparation of 2-(4-bromophenyl)-5,5-dimethyl-2-phenyl-1,3-dioxane (2)

A mixture of 4-bromobenzophenone (**1**) (20.0 g, 0.077 mol), 2,2-dimethylpropane-1,3-diol (12.0 g, 0.1155 mol) and p-TsOH (0.66 g, 0.0038 mol) intoluene (600 mL) was heated at reflux for 18 h with a Dean-Stark trap to remove the H_2O. The reaction mixture was cooled to room temperature and diluted with $CHCl_3$. The organic layer was washed with water and brine, dried over $MgSO_4$, and concentrated in vacuo. The resulting crude product was recrystallized in isopropyl alcohol, yielding 2 (24.2 g, 91%) as a clear crystalline solid; TLC R_f (*n*-hexane:THF = 3:1) 0.75; ^{1}H NMR (600 MHz, $CDCl_3$) δ 0.97 (s, 3H), 1.02 (s, 3H), 3.61 (q, J = 11.19 Hz, 4H), 7.26 (t, J = 7.88, 7.39 Hz, 1H), 7.33 (t, J = 7.64 Hz, 2H), 7.39 (d, J = 8.62 Hz, 2H), 7.44 (d, J = 8.62 Hz, 2H), 7.48 (d, J = 7.16 Hz, 2H); ^{13}C NMR (150 MHz, $CDCl_3$) δ 22.47, 22.57, 30.13, 72.05 (×2), 100.51, 121.89, 126.53 (×2), 127.96, 128.38 (×2), 128.47 (×2), 131.45 (×2), 141.37, 141.43; GC/MS calcd for $C_{18}H_{19}BrO_2$ (M^+): 345.65

Preparation of tetrakis(4-(5,5-dimethyl-2-phenyl-1,3-dioxan-2-yl)phenyl)stannane (3)

Ketal **2a** (15.4 g, 44 mmol), pre-dried by Ar purging, in THF (250 mL) was cooled to 78°C. We added *n*-BuLi (17.6 mL, 44 mmol, 2.5 M in hexane) to the solution dropwise with stirring. After 30 min of stirring tin(IV) chloride (1.00 mL, 8.6 mmol) was added at −78°C. The reaction mixture was stirred for 3 h at −78°C and 12 h at the ambient temperature. The resulting mixture was cooled to room temperature and diluted with $CHCl_3$. The organic layer was washed with 1% aqueous HCl, water, and brine; dried over $MgSO_4$; and concentrated in vacuo. The resulting crude product was recrystallized in ether, yielding **3** (9.136 g, 90%) as a white powder; TLC R_f (*n*-hexane:THF=3:1) 0.50; ^{1}H NMR (600 MHz, $CDCl_3$) δ 0.96 (s, 12H), 0.99 (s, 12H), 3.59 (s, 16H), 7.24 (t, J = 7.89, 6.83 Hz, 4H), 7.32 (t, J = 7.89, 7.37 Hz, 8H), 7.46 (d, J = 8.18 Hz, 8H), 7.48-7.51 (m, 16H); ^{13}C NMR (150 MHz, $CDCl_3$) δ 22.60 (×2), 30.17, 72.09 (×2), 100.86, 126.64 (×2), 126.70 (×2), 127.78, 128.34 (×2), 137.16 (×2), 137.29, 141.73, 142.93; MALDI-TOF MS calcd for $C_{72}H_{76}O_8Sn$ (M^+): 1189.6391.

Preparation of tetrakis(4-benzoylphenyl)stannane (4)

A mixture of tetraketal **3a** (2.00 g, 1.683 mmol) and p-TsOH (0.145 g, 0.842 mol) in acetone (80 mL), THF (80 mL), and H_2O (20 mL) was heated at reflux for 72 h. The reaction mixture was cooled to room temperature and diluted with $CHCl_3$. The organic layer was washed with water and brine, dried over $MgSO_4$, and concentrated in vacuo. The resulting crude product was recrystallized in a 1:3 mixture of THF and *n*-hexane, yielding **4** (1.278 g, 90%) as a clear crystalline solid; TLC Rf (n-hexane:THF = 3:1) 0.28; ^{1}H NMR (600 MHz, $CDCl_3$) δ 7.49 (t, J = 7.41, 8.16 Hz, 8H), 7.61 (t, J = 7.41, 7.51 Hz, 4H), 7.78 (d, J = 8.16 Hz, 8H), 7.80-7.88 (m, 16H); ^{13}C NMR (150 MHz, $CDCl_3$) δ 128.38 (×2), 129.94 (×2), 130.12 (×2), 132.72, 136.97 (×2), 137.17, 138.80, 142.18, 196.52; MALDI-TOF MS calcd for $C_{52}H_{36}O_4Sn$ (M^+): 845.4163.

General procedure for preparation of 6

THF (100 mL) and diethyl benzylphosphonate (7.113 mmol) were added to potassium *tert*-butoxide (10.669 mmol), which was pre-dried by Ar purging. After the solution was stirred for 15 min at the ambient temperature, **4** (0.593 mmol) dissolved in THF (40 mL) was added. The reaction mixture was heated at reflux for 24 h, cooled to room temperature, and diluted with $CHCl_3$. The organic layer was washed with 1% aqueous HCl, water, and brine; dried over $MgSO_4$; and concentrated in vacuo. The resulting crude product was purified by column chromatography.

Tetrakis(4-(1,2-diphenylvinyl)phenyl)stannane (Sn-a) was prepared by the reaction of **4** (0.500 g, 0.593 mmol) with *tert*-butoxide (1.197 g, 10.669 mmol) and diethyl benzylphosphonate (**5a**) (1.489 mL, 7.113 mmol). The crude product was purified by column chromatography, yielding **6a** (0.561 g, 83.0%) as a white powder; TLC R_f (*n*-hexane: THF = 3:1) 0.59; ^{1}H NMR (600 MHz, $CDCl_3$) δ 7.00 - 7.05 (m, 12H), 7.06 - 7.15 (m, 12H), 7.19 - 7.26 (m, 8H), 7.26 - 7.29(m, 4H), 7.30 - 7.43 (m, 16H), 7.51 - 7.62 (m, 8H); ^{13}C NMR (150 MHz, $CDCl_3$) δ 126.82, 127.58, 127.61 (×2), 127.96 (×2), 128.23, 128.66, 129.56 (×2), 130.34, 130.56, 137.05, 137.30, 137.89, 140.16, 141.32, 142.35, 143.14, 144.13; MALDI-TOF MS calcd for $C_{80}H_{60}Sn$ (M^+): 1139.4592.

Tetrakis(4-(1-phenyl-2-(4-tolyl)vinyl)phenyl)stannane (Sn-b) was prepared by the reaction of **4** (0.500 g, 0.593 mmol) with *tert*-butoxide (1.197 g, 10.669 mmol) and diethyl 4-methylbenzylphosphonate (**5b**) (1.595 mL, 7.113 mmol). The crude product was purified by column chromatography, yielding **6b** (0.567 g, 80.0%) as a white powder; TLC R_f (*n*-hexane:THF = 3:1) 0.64; ^{1}H NMR (600 MHz, $CDCl_3$) δ 2.18 - 2.27 (m, 12H), 6.88 - 7.01 (m, 20H), 7.19 - 7.28 (m, 8H), 7.28 - 7.40 (m, 20H), 7.51 - 7.66 (m, 8H); ^{13}C NMR (150 MHz, $CDCl_3$) δ 21.17, 127.39, 127.47, 127.52, 128.21 (×2), 128.71 (×2), 129.47 (×2), 130.34 (×2), 130.56, 134.42, 136.67, 137.05, 137.45, 140.38, 141.45, 143.26, 144.23; MALDI-TOF MS calcd for $C_{84}H_{68}Sn$(M^+): 1195.5623.

Tetrakis(4-(2-(4-*tert*-butylphenyl)-1-phenylvinyl)phenyl) stannane (Sn-c) was prepared by the reaction of **4** (0.500 g,

0.593 mmol) with *tert*-butoxide (1.197 g, 10.669 mmol) and diethyl 4-*tert*-butylbenzylphosphonate (**5c**) (1.960 mL, 7.113 mmol). The crude product was purified by column chromatography, yielding **6c** (0.663 g, 82.0%) as a white powder; TLC R_f (*n*-hexane:THF = 3:1) 0.75; ^{1}H NMR (600 MHz, $CDCl_3$) δ 1.17 - 1.27 (m, 36H), 6.92 - 7.02 (m, 12H), 7.13 - 7.16 (m, 8H), 7.23 - 7.41 (m, 28H), 7.52 - 7.70 (m, 8H); ^{13}C NMR (150 MHz, $CDCl_3$) δ 31.20 (×3), 34.51, 124.93 (×2), 127.41, 127.46, 128.20 (×2), 128.77, 128.80, 129.28 (×2), 130.24, 130.49, 134.31, 137.03, 137.53, 140.43, 141.38, 143.28, 144.24, 149.97; MALDI-TOF MS calcd for $C_{96}H_{92}Sn$ (M^+): 1364.8072.

Tetrakis(4-(2-(1-naphthyl)-1-phenylvinyl)phenyl)stannane (Sn-d) was prepared by the reaction of **4** (0.500 g, 0.593 mmol) with *tert*-butoxide (1.197 g, 10.669 mmol) and diethyl naphthalen-1-ylmethylphosphonate (**5d**) (1.727 mL, 7.113 mmol). The crude product was purified by column chromatography, yielding **6d** (0.579 g, 73.0%) as a white powder; TLC R_f (*n*-hexane:THF = 3:1) 0.46; ^{1}H NMR (600 MHz, $CDCl_3$) δ 6.98 - 7.29 (m, 24H), 7.30 - 7.65 (m, 36H), 7.68 - 7.83 (m, 4H), 8.01 - 8.17 (m, 4H); ^{13}C NMR (150 MHz, $CDCl_3$) δ 124.61, 125.23, 125.73, 125.97, 126.63, 127.18, 127.72, 128.06, 128.17, 128.28, 128.46, 130.64, 132.49, 133.43, 135.06, 136.53, 136.79, 137.10, 137.45, 139.99, 141.06, 143.11, 143.98, 144.55; MALDI-TOF MS calcd for $C_{96}H_{92}Sn(M^+)$: 1339.6542.

Tetrakis (4-(2-(4-biphenyl)-1-phenylvinyl)phenyl)stannane (Sn-e) was prepared by the reaction of **4** (0.500 g, 0.593 mmol) with *tert*-butoxide (1.197 g, 10.669 mmol) and diethyl 4-biphenylphosphonate (**5e**) (2.165 g, 7.113 mmol). The crude product was purified by column chromatography, yielding **6e** (0.582 g, 68.0%) as a white powder; TLC R_f (*n*-hexane:THF = 3:1) 0.44; ^{1}H NMR (600 MHz, $CDCl_3$) δ 7.00 - 7.04 (m, 4H), 7.06 - 7.11 (m, 8H), 7.22 - 7.42 (m, 48H), 7.43 - 7.56 (m, 8H), 7.56 - 7.70 (m, 8H); ^{13}C NMR (150 MHz, $CDCl_3$) δ 126.56 (×2), 126.78, 126.82 (×2), 127.23, 127.58 (×2), 128.26, 128.71 (×2), 128.79, 130.03 (×2), 130.32, 130.60, 136.29, 137.09, 137.49, 139.36, 140.20, 140.55, 141.40, 142.45, 143.09, 144.15; MALDI-TOF MS calcd for $C_{104}H_{76}Sn$ (M^+): 1443.7462.

2.3 OLED fabrication and measurement

An OLED device was fabricated on a glass substrate coated with indium tin oxide (ITO, 150 nm thick, ~20 Ω/sq). The samples were cleaned in sequence with acetone, isopropyl alcohol, and deionized water and then dried with high-purity nitrogen gas. Next, they were pretreated with UV/ozone radiation to increase their work function.[24] The structure of the OLED devices comprised ITO/poly(3,4-ethylenedioxythiophene) poly(styrenesulfonate) (PEDOT:PSS) and (40 nm)/N,N′-Di(1-naphthyl)-N,N′-diphenyl-(1,1′-biphenyl)-4,4′-diamine (NPB, 30 nm)/synthesized tin-cored material (30 nm)/bathocuproine (BCP, 30 nm)/LiF (1 nm)/Al (100 nm). As a hole-injection layer (HIL), the PEDOT:PSS was spin-coated and annealed at 150°C for 15 min in ambient air. The NPB, synthesized tin-cored material, and BCP were deposited as a hole transport layer, an emitting layer, and an electron-transport and hole-blocking layer, respectively, under a vacuum of ~5×10^{-6} Torr at a deposition rate of 1 Å/s. LiF and Al were then deposited in a vacuum chamber at rates of 0.1 and 10 Å/s, respectively. Five different types of devices were fabricated in order to investigate the effects of the tetrahedral structure and functional groups on the performance of the OLEDs. A Keithley 2622A source meter and a MINOLTA CS100A luminance meter were used to measure the current-voltage luminance characteristics and Commission Internationale de l'Eclairage (CIE) chromaticity coordinates.

3. RESULTS AND DISCUSSION

3.1 Material properties

The optical properties of the synthesized compounds obtained through UV-Vis absorption and PL spectroscopy are shown in Fig. 2. The intensity is normalized in the figure. The maximum absorption wavelengths of Sn-a, Sn-b, Sn-c, Sn-d, and Sn-e in chloroform appeared at 308, 312, 313, 330, and 328 nm, respectively, and are associated with π-π* transitions.[25] The adsorption edges (λ_{edge}) were determined by extrapolating two solid lines from the background and straight onset in the spectra. The adsorption edges of Sn-a, Sn-b, Sn-c, Sn-d, and Sn-e were 348, 354, 354, 377, and 372 nm, respectively. The optical bandgap (E_g) was calculated using λ_{edge} according to the equation $E_g = 1240/\lambda_{edge}$, which corresponds to 3.56, 3.50, 3.50, 3.28, and 3.33 eV for Sn-a, Sn-b, Sn-c, Sn-d, and Sn-e, respectively. The aromatic substituents appear to reduce the bandgap by a larger amount than the aliphatic substituents. The maximum PL emission wavelengths of the compounds in the chloroform were in the range of 429 - 448 nm, as shown in Fig. 2(b). The emission peaks of Sn-b, Sn-c, Sn-d, and Sn-e exhibited bathochromic shifts compared with that of Sn-a, indicating that the methyl, *tert*-butyl, naphthyl and phenyl substituents furthered the conjugation of the compounds.[26] Figure 2(c) shows the normalized PL spectra of the compounds in the solid state. The main peak positions of the PL spectra were measured to be 422, 421, 420, 424, and 435 nm for Sn-a, Sn-b, Sn-c, Sn-d, and Sn-e, respectively.

To understand the thermal behavior and thermal stability of the synthesized Sn-cored materials, thermogravimetric analysis was performed in the range of 30 - 800°C. As shown in Fig. 3, the reaction started near 400°C regardless of sample types. The weight loss processed sharply until 500°C for Sn-a, Sn-b, and Sn-c, and 520°C for Sn-d and Sn-e. After these temperature, the decomposition process slowed down. The total weight losses until the decomposition reaction

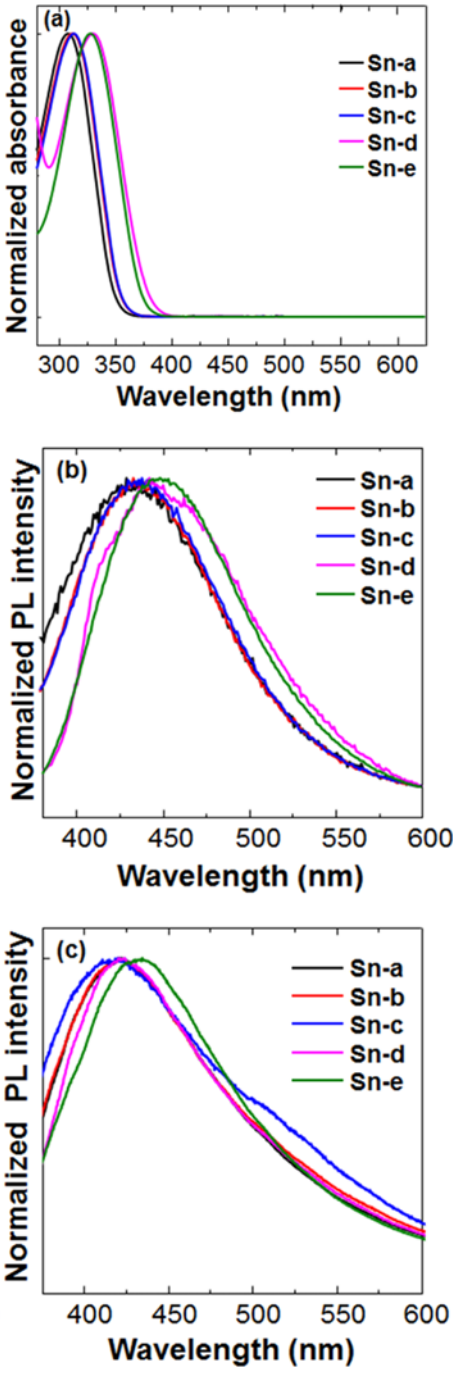

Fig. 2. (a) UV-Vis absorption spectra of synthesized compounds. (b) PL spectra of synthesized compounds in solution. (c) PL spectra of synthesized compounds in film.

process slowed down were 70, 57, 78, 70, and 65% for Sn-a, Sn-b, Sn-c, Sn-d, and Sn-e, respectively.

Figures 4(a)-(e) present the secondary cutoff spectra and valence-band spectra for each compound. The onset of the secondary electrons and valence-band maximum was determined by extrapolating two solid lines from the

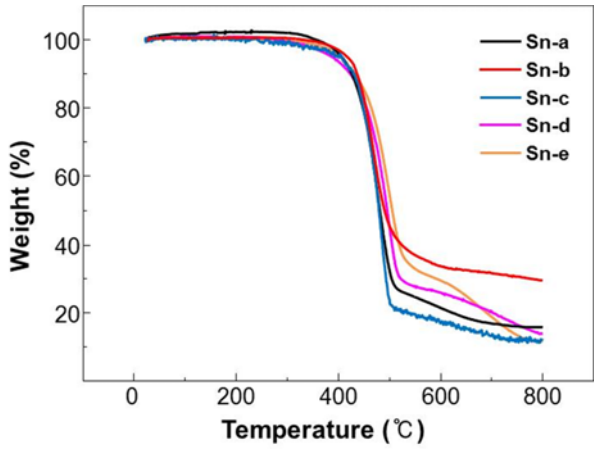

Fig. 3. Thermogravimetirc analysis data of synthesized compounds.

background and the straight onset in the spectra.[27] The work-function and valence-band maxima for the compounds were measured to be 4.75 and 1.1 eV for Sn-a, 4.9 and 0.6 eV for Sn-b, 5.0 and 0.7 eV for Sn-c, 4.75 and 0.9 eV for Sn-d, and 4.6 and 1.1 eV for Sn-e. The position of the valence-band maximum represents the energy-level difference between the highest occupied molecular orbital (HOMO) and the Fermi level. Thus, the HOMO levels were calculated by the summation of the work function and the valence band maximum. Furthermore, the lowest unoccupied molecular orbital (LUMO) levels were calculated by the subtraction of E_g from the HOMO. Table 1 summarizes the main peak positions of the UV absorption, PL spectra in solution, and PL spectra in the solid state, as well as the HOMO and LUMO levels of the compounds and the calculated Eg. These results suggest that synthesized Sn-cored compounds can be used as the emitting layer of blue OLEDs.

Figures 5(a)-(e) show the changes in the PL intensity with respect to the water fraction (F_w) in THF-water mixtures. Clearly, the PL intensity of each compound that dissolved in the THF-water mixtures increased with the F_w. The change in the PL intensity in THF-water mixture (I) with respect to the PL intensity in the THF (I_0) is summarized in Fig. 5(f). For Sn-e, the PL intensity was dramatically enhanced over 554-fold as the F_w increased from 0 to 90%. Interestingly, the bathochromic shifts of the emission peaks in Sn-b, Sn-c, Sn-d, and Sn-e compared with that of Sn-a remained in the THF-water mixtures. Images of Sn-cored organic compounds in THF and the THF-water mixture under illumination by a UV lamp are shown in the inset of Figs. 5(a)-(e). The Sn-cored materials aggregated in the THF-water mixture because of the non-dissolved property of their molecules in water. Generally, planar luminophoric molecules aggregate as discs pile up, owing to the strong π-π stacking interactions between the aromatic rings. This kind of aggregation induced quenching, which commonly turns off the light

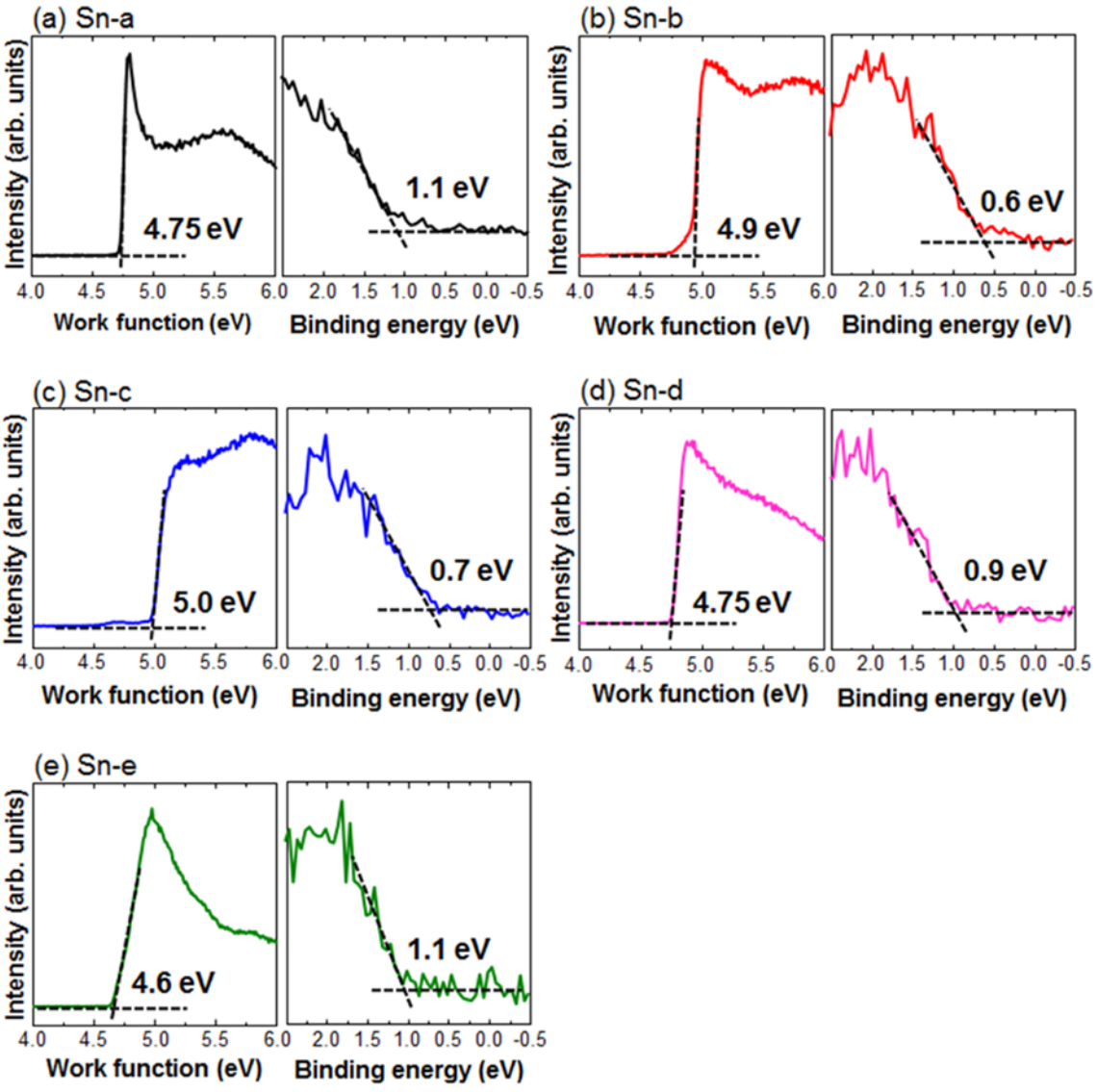

Fig. 4. Secondary cutoff spectra and valence-band spectra of (a) Sn-a, (b) Sn-b, (c) Sn-c, (d) Sn-d, and (e) Sn-e. The onset of the secondary electrons and valence-band maximum was determined by extrapolating two solid lines from the background and the straight onset in the spectra.

Table 1. Optical and electrochemical properties of the synthesized materials.

Materials	UV_{max} (nm)	PL_{max} (nm)		HOMO (eV)	LUMO (eV)	E_g (eV)
	Solution	Solution	Film			
Sn-a	308	429	422	5.75	2.19	3.56
Sn-b	312	433	421	5.5	2.0	3.50
Sn-c	313	438	420	5.7	2.2	3.50
Sn-d	330	442	424	5.65	2.37	3.28
Sn-e	328	448	435	5.7	2.37	3.33

emission.[28] However, the aggregation of Sn-cored materials, which comprise nonplanar luminophoric molecules, increased the emission similarly to AIE molecules.[29,30] The intermolecular rotations appeared to be restricted by the steric constraint. Thus, the non-radiative relaxations are blocked and the radiative decays are boosted by the restriction of intermolecular rotations in non-planar Sn-cored materials.

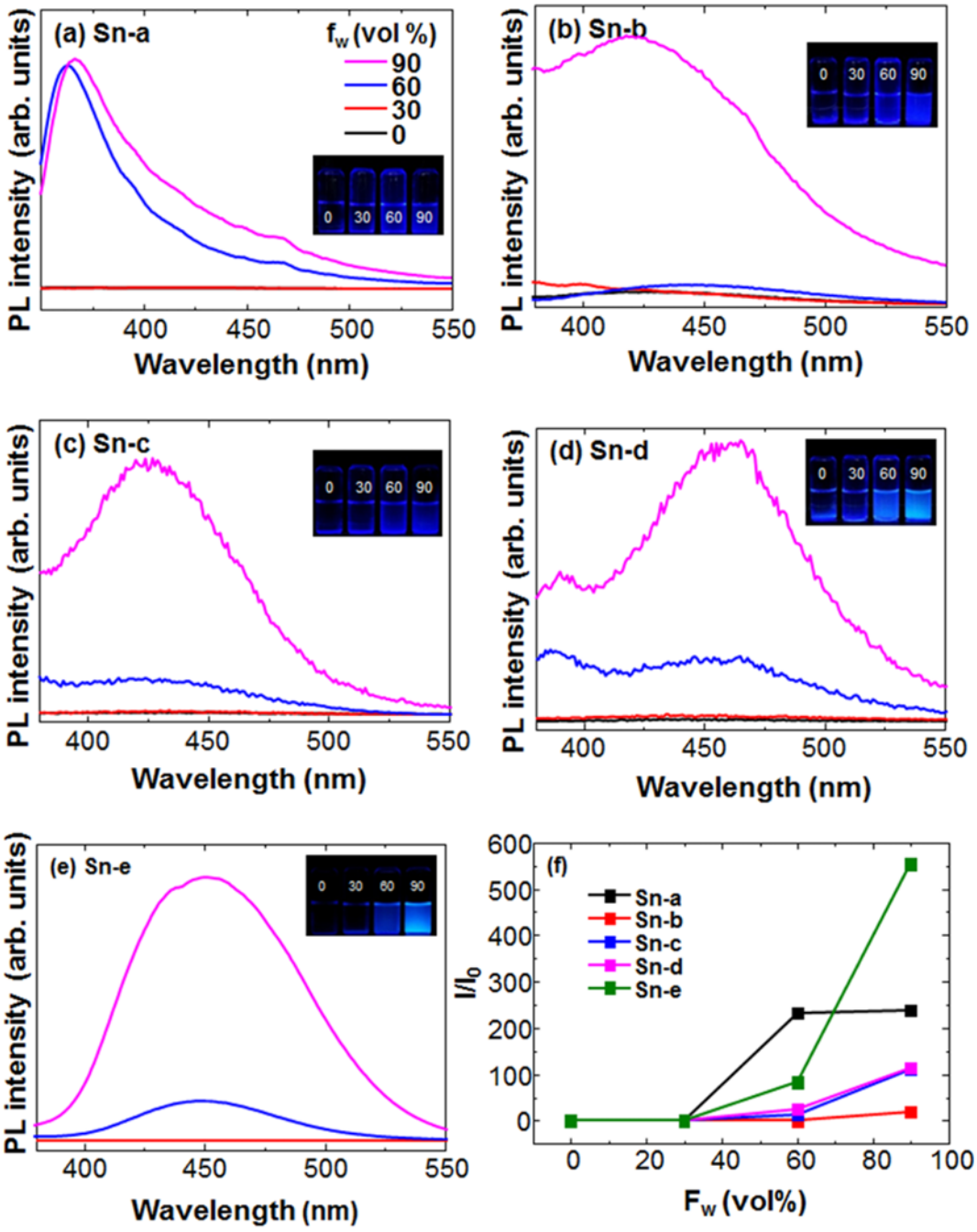

Fig. 5. Changes in the PL intensity for (a) Sn-a, (b) Sn-b, (c) Sn-c, (d) Sn-d, and (e) Sn-e with different water fractions in the THF-water mixtures. (f) A summary of the change in the PL intensity in THF-water mixture (I) with respect to the PL intensity in THF (I_0).

Figure 6(a) shows the 2D-GIXD images of Sn-cored materials thermally deposited on a Si substrate. The diffraction peak in the out-of-plane direction was observed in Sn-a, Sn-b, and Sn-c samples, indicating side-chain packing. However, no peak was observed in Sn-d or Sn-e. For a detailed characterization, the out-of-plane and in-plane diffraction profiles are shown in Figs. 6(b) and (c). The peaks of Sn-a, Sn-b, and Sn-c were observed at q_z = 0.44, 0.45, and 0.39 $Å^{-1}$, indicating side-chain packing distances of 14.28, 14.12, and 15.95 Å, respectively. No peaks were observed in the in-plane diffraction profiles, regardless of the substituents, suggesting that π-π stacking is not due to the tetrahedral structure. Therefore, it is considered that the tetrahedral structure of Sn-cored organic compounds with methyl or *tert*-butyl substituents cannot prevent side-chain packing. However, naphthyl and phenyl substituents in a

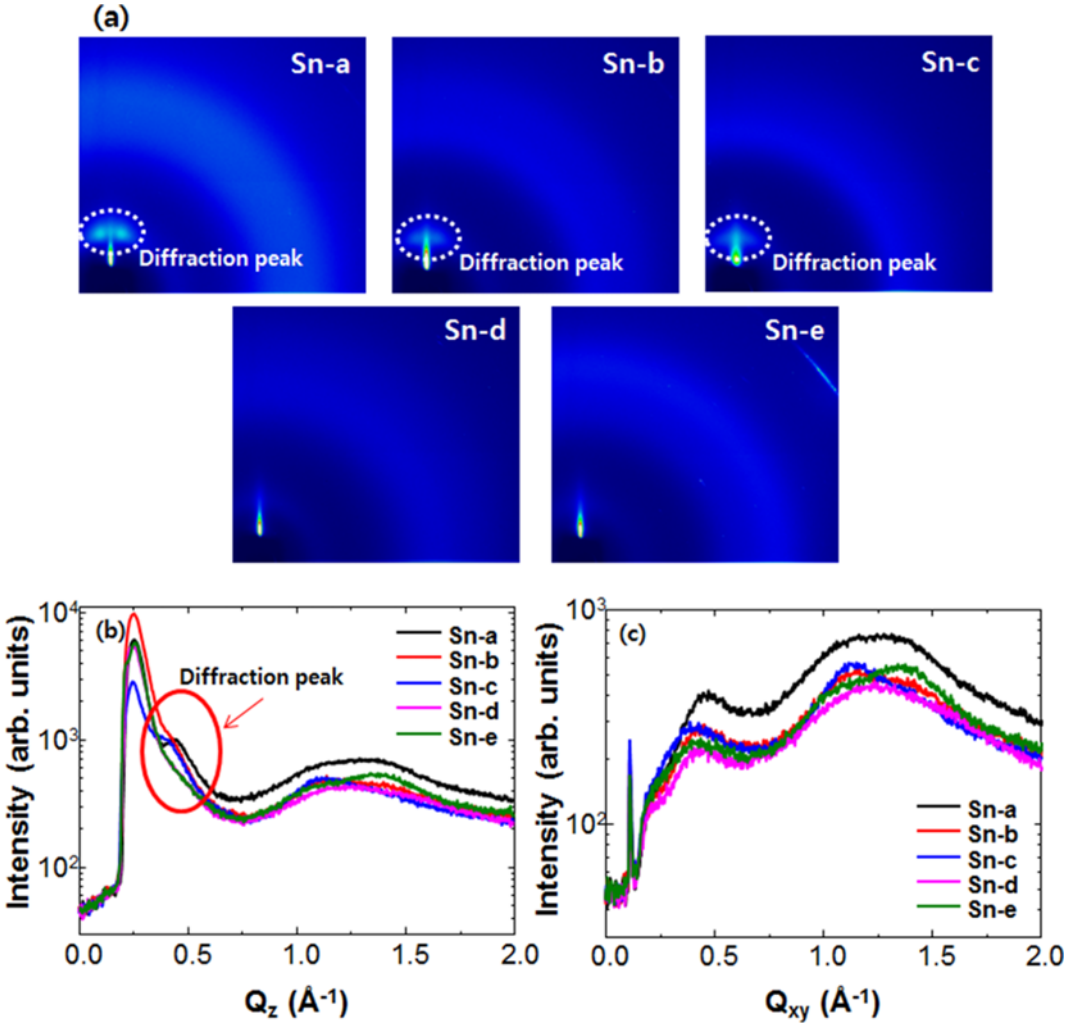

Fig. 6. (a) 2D-GIXD images of Sn-cored materials. (b) Out-of-plane and (c) in-plane diffraction profiles.

tetrahedral structure of Sn-cored organic compounds can prevent side-chain packing as well as π-π stacking. We consider that aromatic substituents are more appropriate than aliphatic ones for prohibiting side-chain packing and π-π stacking in the tetrahedral structures of Sn-cored organic compounds. These results indicate that the thermal deposition of Sn-cored materials formed a suitable condensed state.

3.2 OLED characteristics

Figure 7 shows the (a) current density-voltage, (b) luminance-voltage, (c) luminance efficiency-current density, and (d) power efficiency-current density characteristics of the OLED devices using Sn-cored materials as an emitting layer. The device structure is shown in the inset of Fig. 7(a). The HOMO and LUMO levels were 5.5 and 2.4 eV for NPB and 6.5 and 3.0 for BCP.[31] As shown in Table 1, the measured HOMO and LUMO levels of Sn-cored compounds were 5.5 - 5.75 eV and 2.0 - 2.37 eV, respectively, which are adequate for the use of Sn-cored materials as emitting layers in OLED devices. The turn-on voltages at 10 cd/m^2 were 6.75 - 8 V. The Sn-e based device exhibited the highest luminance value of 602 cd/m^2. The inset of Fig. 7(b) shows an OLED device after the voltage was applied. The maximum luminance efficiencies and power efficiencies were measured to be 0.67 cd/A and 0.26 lm/W; 0.71 cd/A and 0.28 lm/W; 0.39 cd/A and 0.15 lm/W; 0.38 cd/A and 0.18 lm/W; and 0.58 cd/A and 0.21 lm/W for the Sn-a, Sn-b, Sn-c, Sn-d, and Sn-e-based OLEDs, respectively. The difference of device characteristics is not much according to the substituents in the Sn-cored materials, as shown in Table II, even though AIE characteristics of the Sn-cored materials are different depending on the substituents. It is considered that many factors determine the device characteristics including AIE, energy level alignment, internal quantum efficiency of active layer, and so on. These results indicate that Sn-cored compounds can be used as emitting layers in

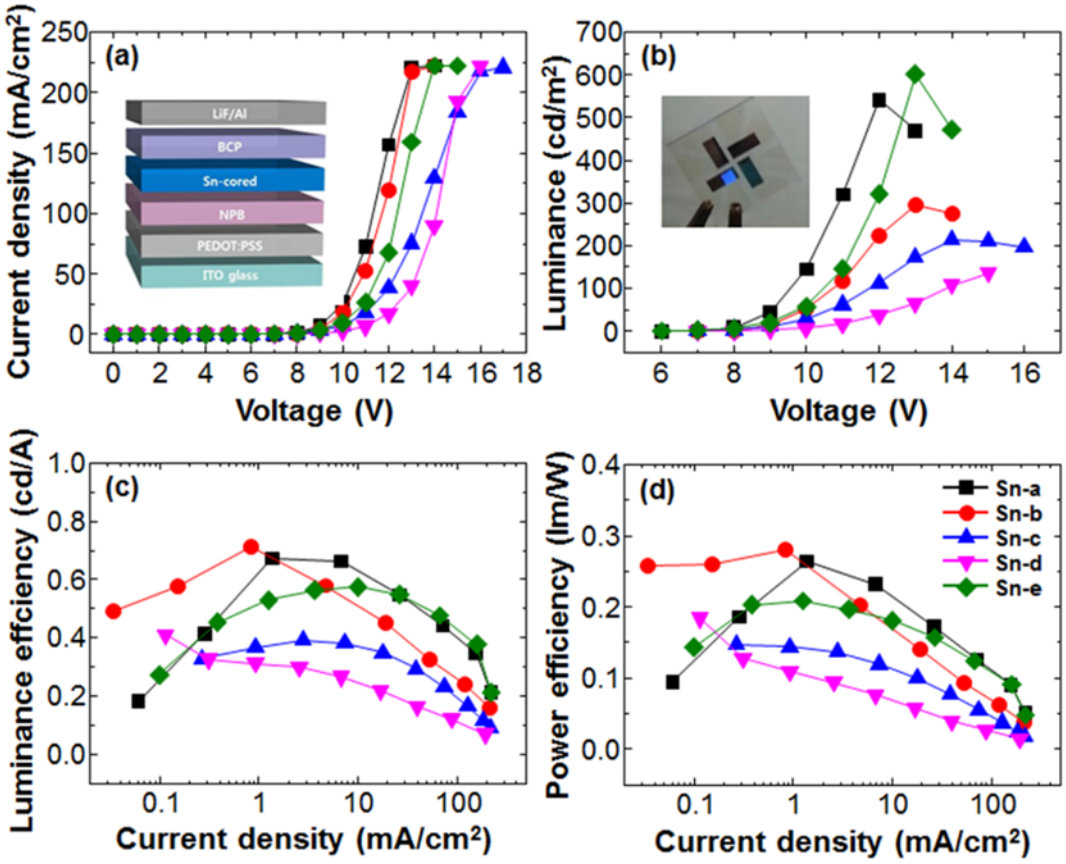

Fig. 7. (a) Current density-voltage, (b) luminance-voltage, (c) luminance efficiency-current density, and (d) power efficiency-current density characteristics of the OLED devices using Sn-cored materials as an emitting layer. The device structure is shown in the inset of Fig. 6(a). The inset of Fig. 6(b) shows an OLED device after the voltage was applied.

Table 2. Summary of OLED characteristics.

Materials	V_{on} a)	L^{max} b)	LE^{max} c)	PE^{max} d)	EL^{max} e)	CIE f)
Sn-a	6.95	541	0.67	0.26	440	(0.15, 0.11)
Sn-b	7	296	0.71	0.28	456	(0.155, 0.10)
Sn-c	7.15	215	0.39	0.15	443	(0.158, 0.144)
Sn-d	8	136	0.38	0.18	451	(0.205, 0.24)
Sn-e	6.75	602	0.58	0.21	474	(0.176, 0.20)

[a] V_{on} : Turn-on voltage at 10 cd/m^2 [V]
[b] L^{max} : Luminance^{max} [cd/m^2]
[c] LE^{max} : Luminance Efficiency^{max} [cd/A]
[d] PE^{max} : Power Efficiency^{max} [lm/W]
[e] EL^{max} : Electroluminescence (nm)
[f] CIE : CIE coordinates [x, y]

blue OLEDs.

Figures 8(a) and (b) show the electroluminescence spectra and CIE chromaticity color coordinates of the OLEDs based on Sn-cored compounds. The electroluminescence peak position and CIE color coordinates were measured as 440 nm and (0.150, 0.110); 456 nm and (0.155, 0.100); 443 nm and (0.158, 0.144); 451 nm and (0.205, 0.240); and 474 nm and (0.176, 0.200) for the Sn-a, Sn-b, Sn-c, Sn-d, and Sn-e-based OLEDs, respectively. These results indicate that aromatic functional groups increase the coordination of x and y in the CIE, compared with aliphatic functional groups.

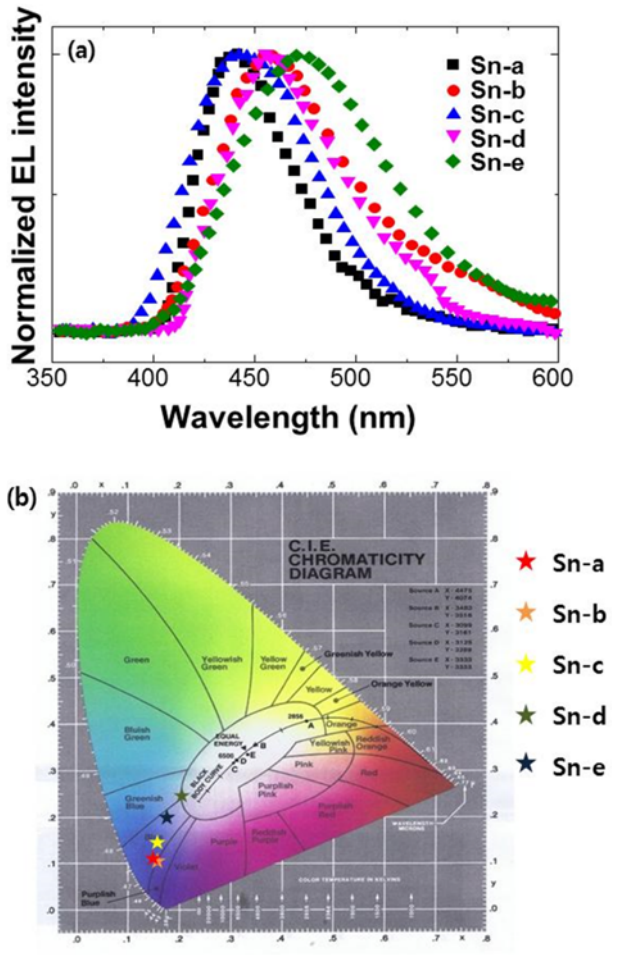

Fig. 8. (a) Electroluminescence spectra and (b) CIE chromaticity color coordinates of the Sn-cored compound-based OLEDs.

4. CONCLUSIONS

Tetrahedral structures comprising Sn-cored materials were synthesized, characterized, and applied to blue OLEDs. For substituents of the Sn-cored tetrahedral stilbenoids, methyl and *tert*-butyl were used as aliphatic groups, and naphthyl and phenyl were used as aromatic groups. UV-Vis absorption spectra showed that the bandgap of the Sn-cored tetrahedral stilbenoids was in the range of 3.28 - 3.56 eV. The aromatic substituents appeared to reduce the bandgap more than the aliphatic substituents. The PL emission peaks of Sn-b (433 nm), Sn-c (438 nm), Sn-d (442 nm), and Sn-e (448 nm) in a dilute solution were bathochromically shifted compared with that of Sn-a (429 nm) owing to the increase in the conjugation of the compounds. The PL emission peak intensities of the Sn-cored materials in THF-water mixture were dramatically enhanced 21 to 554-fold as the F_w increased from 0 to 90%, indicating that Sn-cored materials had AIE characteristics. According to the 2D-GIXD data, aromatic substituents are more appropriate than aliphatic ones for prohibiting side-chain packing and π-π stacking in tetrahedral structures of Sn-cored organic compounds. The measured HOMO and LUMO levels of the Sn-cored compounds were 5.5 - 5.75 eV and 2.0 - 2.37 eV, respectively, which are adequate for the use of Sn-cored materials as emitting layers in OLED devices. The maximum luminance efficiencies and power efficiencies of the Sn-cored compound-based OLEDs were 0.38 - 0.71 cd/A and 0.15 - 0.28 lm/W, respectively. The device characteristics were similar regardless of the substituents in the Sn-cored materials. However, CIE coordination data showed that the aromatic functional groups increased the coordination of x and y in the CIE compared with the aliphatic functional groups. Therefore, we consider that tetrahedral structures of Sn-cored compounds-particularly those with aromatic substituents-can be used as active materials in blue OLEDs for prohibiting side-chain packing and π-π stacking.

ACKNOWLEDGEMENTS

This research was supported in part by the National Research Foundation of Korea (NRF) grant provided by the Korean government (MSIP) (No. 2014R1A2A1A11051098) and in part by the International Cooperative R&D program through the Korea Institute for Advancement of Technology (KIAT) funded by the Ministry of Trade, Industry, and Energy (MOTIE) of Korea.

REFERENCES

1. H. Sasabe and J. Kido, *J. Mater. Chem. C* **1**, 1699 (2013).
2. J. Wang, F. Zhang, J. Zhang, W. Tang, A. Tang, H. Peng, Z. Xu, F. Teng, and Y. Wang, *J. Photoch. Photobio. C* **17**, 69 (2013).
3. J. H. Kim, J.-Y. Cho, J. Park, B. K. Lee, K.-H. Baek, H. Lee, and L.-M. Do, *Electron. Mater. Lett.* **10**, 27 (2014).
4. G.-P. Kim, B.-M. Park, and H.-J. Chang, *Electron. Mater. Lett.* **10**, 491 (2014).
5. N.-C. Seong, Y.-M. Jeon, T.-H. Lim, J.-W. Kim, C.-W. Lee, E.-J. Lee, J.-G. Jang, H.-J. Jang, J.-Y. Lee, and M.-S. Gong, *Synthetic Met.* **157**, 421 (2007).
6. L. Xiao, Z. Chen, B. Qu, J. Luo, S. Kong, Q. Gong, and J. Kido, *Adv. Mater.* **23**, 926 (2011).
7. K. S. Choi, H. Jo, K. Park, S. Y. Kim, B. H. Koo, K. Hong, and J.-L. Lee, *J. Phys. Chem. C* **115**, 9767 (2011).
8. Y. Wei and C.-T. Chen, *J. Am. Chem. Soc.* **129**, 7478 (2007).
9. H.-C. Yeh, R.-H. Lee, L.-H. Chan, T.-Y. J. Lin, C.-T. Chen, E. Balasubramaniam, and Y.-T. Tao, *Chem. Mater.* **13**, 2788 (2001).
10. S. Wang, W. J. Oldham, R. A. Hudack, and G. C. Bazan, *J. Am. Chem. Soc.* **122**, 5695 (2000).
11. S.-K. Kim, Y.-I. Park, I.-N. Kang, and J.-W. Park, *J. Mater.*

Chem. **17**, 4670 (2007).
12. S. Liu, F. He, H. Wang, H. Xu, C. Wang, F. Li, and Y. Ma, *J. Mater. Chem.* **18**, 4802 (2008).
13. S.-C. Lo and P. L. Burn, *Chem. Rev.* **107**, 1097 (2007).
14. P. Furuta, J. Brooks, M. E. Thompson, and J. M. J. Fréchet, *J. Am. Chem. Soc.* **125**, 13165 (2003).
15. X.-M. Liu, C. He, X.-T. Hao, L.-W. Tan, Y. Li, and K. S. Ong, *Macromolecules* **37**, 5965 (2004).
16. Q. He, H. Huang, Q. Sun, H. Lin, J. Yang, and F. Bai, *Polym. Advan. Technol.* **15**, 43 (2004).
17. Y.-Y. Lyu, J. Kwak, W. S. Jeon, Y. Byun, H. S. Lee, D. Kim, C. Lee, and K. Char, *Adv. Funct. Mater.* **19**, 420 (2009).
18. Y. Park, K. S. Choi, S. Y. Kim, H. Jo, and K. Park, *Displays* **33**, 55 (2012).
19. Z. Zhao, S. Chen, X. Shen, F. Mahtab, Y. Yu, P. Lu, J. W. Lam, H. S. Kwok, and B. Z. Tang, *Chem. Commun.* **46**, 686 (2010).
20. W. Z. Yuan, P. Lu, S. Chen, J. W. Lam, Z. Wang, Y. Liu, H. S. Kwok, Y. Ma, and B. Z. Tang, *Adv. Mater.* **22**, 2159 (2010).
21. Y. Hong, J. W. Y. Lam, and B. Z. Tang, *Chem. Soc. Rev.* **40**, 5361 (2011).
22. R. Hu, N. L. Leung, and B. Z. Tang, *Chem. Soc. Rev.* **43**, 4494 (2014).
23. J. Mei, Y. Hong, J. W. Lam, A. Qin, Y. Tang, and B. Z. Tang, *Adv. Mater.* **26**, 5429 (2014).
24. C. Kim, T. P. Nguyen, Q. V. Le, J.-M. Jeon, H. W. Jang, and S. Y. Kim, *Adv. Funct. Mater.* **25**, 4512 (2015).
25. K. Guo, Z. Gao, J. Cheng, Y. Shao, X. Lu, and H. Wang, *Dyes Pigments* **115**, 166 (2015).
26. C. Liu, W. He, G. Shi, H. Luo, S. Zhang, and Z. Chi, *Dyes Pigments* **112**, 154 (2015).
27. K. C. Kwon, C. Kim, Q. V. Le, S. Gim, J.-M. Jeon, J. Y. Ham, J.-L. Lee, H. W. Jang, and S. Y. Kim, *ACS Nano* **9**, 4146 (2015).
28. Z. Zhang, Y. Zhao, R. Zhang, L. Zhang, W. Cheng, and Z. H. Ni, *Dyes Pigments* **118**, 95 (2015).
29. H. Shi, W. Zhang, X. Dong, X. Wu, Y. Wu, L. Fang, Y. Miao, and H. Wang, *Dyes Pigments* **104**, 34 (2014).
30. L. Chen, Y. Jiang, H. Nie, P. Lu, H. H. Y. Sung, I. D. Williams, H. S. Kwok, F. Huang, A. Qin, Z. Zhao, and B. Z. Tang, *Adv. Funct. Mater.* **24**, 3621 (2014).
31. C. Y. Lee, Q. V. Le, C. Kim, and S. Y. Kim, *Phys. Chem. Chem. Phys.* **17**, 9369 (2015).